Available online at www.sciencedirect.com
ScienceDirect
Cement and Concrete Research 36 (2006) 1434–1443
Cement and Concrete Research

# The microstructure of concrete made with municipal waste incinerator bottom ash as an aggregate component

Urs Müller *, Katrin Rübner

*Federal Institute for Materials Research and Testing (BAM), Division VII.1-Building Materials, Unter den Eichen 87, D-12205 Berlin, Germany*

Received 18 August 2005; accepted 23 March 2006

**Abstract**

The interaction of municipal solid waste incinerator bottom ash (MSWI bottom ash), when utilized as an aggregate in concrete, with the cement matrix was investigated. The most prominent reaction observed in lab and field concrete was the formation of aluminium hydroxide and the release of hydrogen gas from aluminium grains reacting in the alkaline environment. The expansive aluminium reaction was identified as a main cause of extensive spalling on the concrete surface. Due to the higher content of bottle glass as part of the ash, in all samples, reaction products of an alkali-silica reaction (ASR) could be observed as well. However, damage due to ASR were less severe than those caused by the aluminium reaction. The expansion rates were low and only a few of the lab samples showed cracking. Microstructural analysis of the samples indicated clearly that a large quantity of the alkali-silica gel which was formed was accommodated in the pores and voids without exerting any strain on the material.


*Keywords:* Microstructure; Alkali-aggregate reaction; Durability; Concrete; Waste management

## 1. Introduction

The incineration of municipal solid waste is becoming increasingly important for waste management because of the new European regulations which prohibit storing of untreated waste in landfills. Research concerning the use of residues from waste incinerators in concrete production is therefore a positive advance in sustainable development, by saving natural resources and decreasing waste volume stored in landfills. Today, modern reprocessing techniques lead to incinerator slag or ashes, which have the potential to be used as aggregates or mineral additions in cementitious building materials. Because of a highly sophisticated reprocessing technique residues with relatively stable composition, relatively well defined properties, and with contents of harmful components, (such as heavy metals and hydrocarbons) below legal limits, can be produced. Attempts are being made to custom design material properties according to their application by varying reprocessing methods.

In recent years many studies were performed in order to find possibilities for incorporating municipal solid waste incinerator bottom ashes (MSWI bottom ashes) into building materials or structures. MSWI bottom ash is now widely used in road construction as a gravel material in compacted base layers [1–4]. Appendino et al. [5] demonstrated that bottom ashes can also be sintered together with other waste materials, to form glass-ceramic bodies, with possible applications as tile or brick material. For cement based materials MSWI bottom ash was studied as a possible mineral addition [6–9] or as a constituent raw material for cement production [10–14].

MSWI bottom ash was considered as an aggregate component of concrete for some time. The first attempts at dealing with technological and physical properties of fresh and hardened concrete, together with chemical analyses, generally show the potential to use bottom ash as an aggregate material [15–18]. The present paper is part of an ongoing study which investigates the effects and performance of MSWI bottom ash aggregates in concrete, and focuses on the microstructural aspects of this material in interaction with the cement paste. The main goal was therefore to analyze reactions occurring between

* Corresponding author.
*E-mail address:* urs.mueller@bam.de (U. Müller).

0008-8846/$ - see front matter © 2006 Elsevier Ltd. All rights reserved.
doi:10.1016/j.cemconres.2006.03.023

the ash constituents and the cementitious binder on a microlevel and, its possible impact on the performance and durability of the concrete.

## 2. Materials and methods

### 2.1. Analyzed bottom ash and concrete specimens

The bottom ash originated from a waste incineration and processing plant in Northern Germany. It consisted of 80% mineral components, such as glassy, crystalline silicates, aluminates and oxides, and 15% bottle glass, as well as metals, ceramics (china, bricks, etc.) and organic residues each with an amount of about 2% (Fig. 1). The chemical composition of the MSWI bottom ash is shown in Table 1. The chemical properties of the bottom ash concerning its use as an aggregate were determined according to DIN EN 1744-1 [19]. The results are listed in Table 2. Calcium hydroxide, as described by many authors (e.g. [21,22]) could not be detected by XRD, but calcium carbonate could be detected as a minor component.

In total, three different groups of concretes were investigated. Two sets of samples were prepared in our labs. The mixture proportions and some of the concrete properties are listed in Table 3. Concretes were made with ordinary Portland cement (CEM I 32,5 R). Aggregates according to the grading curve of B32 were used. The aggregates contained natural sand and gravel as well as MSWI bottom ash with a particle size range of 2–8 mm or 2–32 mm (instead of gravel). These concretes showed characteristic 28 day strengths of about 25 MPa. Their total porosity was double that of the reference concrete (total porosity was calculated from apparent density and true density). One set of concrete was analyzed after water storage for several weeks. The other sets were exposed in a humidity chamber at 40 °C and 99.9% r.h. for 9 months, where expansion and condition of the specimens were recorded at predefined time intervals (according to the German guideline for testing concrete on ASR [20]).

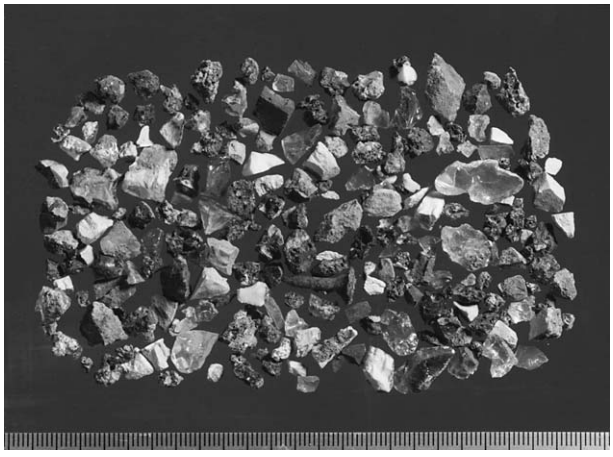

Fig. 1. The crushed 16–32 mm fraction of the MSWI bottom ash with mineral components, bottle glass, metal and ceramic.

Table 1
Avarege chemical composition of MSWI bottom ash

| Component | $SiO_2$ | CaO | MgO | $Al_2O_3$ | $Fe_2O_3$ | CuO | ZnO | $Na_2O$ | $K_2O$ | $SO_3$ |
|---|---|---|---|---|---|---|---|---|---|---|
| Amount (M-%) | 55.7 | 11.9 | 2.7 | 14.1 | 8.8 | 0.5 | 0.3 | 1.4 | 1.2 | 0.7 |

The third set of samples consisted of drilled cores of concrete beams which were exposed outdoors for a total period of 8 years. The specimens were cast on site with steel reinforcements and rested on a footing with drainage. These specimens contained bottom ash with a maximum size of 32 mm.

All concrete specimens, field samples as well as the laboratory concretes, exhibited a similar visual appearance. The surfaces were always pitted or cratered. Some of the laboratory and all of the outdoor specimens showed spalling, which usually consisted of cone shaped detachments. The dip of the cone pointed towards a grain, located in or nearby to, the centre of the affected area (Fig. 2). Spalling appeared also around edges or corners of the laboratory samples (Fig. 3).

### 2.2. Analytical methods

The microstructure of the concrete specimens was analyzed by microscopic methods. Thin section and polished cross sections from $50 \times 50$ to $100 \times 75$ $mm^2$ in size were first analyzed by petrographic microscopy. For higher resolutions a Scanning Electron Microscope (SEM) with a field emission gun was utilized. The SEM analysis was performed under low vacuum mode with a low nitrogen pressure. Microchemical analysis was carried out by a micro X-ray fluorescence spectrometer (MXRF) and by the EDX system attached to the SEM. The MXRF technique was used to acquire large scale elemental maps and to determine the qualitative cross chemical composition of a particular sample area [23]. SEM–EDX

Table 2
Chemical properties of MSWI bottom ash determined according to DIN EN 1744-1 [19]

| Component amount in M-% | Fraction of MSWI bottom ash | | |
|---|---|---|---|
| | 2–8 mm | 8–16 mm | 16–32 mm |
| Acid soluble chloride | 1.59 | 1.60 | 1.58 |
| Water soluble chloride | 0.49 | 0.49 | 0.50 |
| Acid soluble sulfate [a] | 0.80 | 0.48 | 0.52 |
| Water soluble sulfate [a] | 0.03 | 0.02 | 0.02 |
| Total sulfate [a] | 0.82 | 0.49 | 0.55 |
| NaOH sensitive components [b] | 3.10 | 4.17 | 0.94 |
| Aluminum | 1.0 | 0.7 | 0.3 |
| Floating components | 8.73 | 5.88 | 4.97 |
| Organic components [c] | + | – | – |
| Water solubility | 0.75 | 0.42 | 0.31 |
| Loss of ignition | 1.10 | 0.94 | 0.85 |
| Free CaO | 3.24 | 3.24 | 2.88 |

[a] Calculated as $SO_3$.
[b] Glass, Al, Fe, Zn, organic compounds, alkali sensitive mineral phases.
[c] Color in comparison to a colored reference solution (+=darker, −=lighter).

Table 3
Mixture proportions and properties of the laboratory concretes

| | Reference concrete (without bottom ash) | With bottom ash 2–8 mm | With bottom ash 2–32 mm |
|---|---|---|---|
| Cement content kg/m$^3$ | 310 | 310 | 310 |
| Aggregate content kg/m$^3$ | 1828 | 1726 | 1662 |
| Grading curve | B 32 | B 32 | B 32 |
| W/c total | 0.60 | 0.65 | 0.76 |
| W/c effective | 0.60 | 0.60 | 0.60 |
| Slump mm | 480 | 480 | 480 |
| Total porosity % | 11.7 | 17.0 | 22.5 |
| Compressive strength (28 days) MPa | 36.2 | 28.1 | 24.4 |

analysis was used if higher resolutions were necessary. Additional information concerning the phase composition of the MSWI ash was acquired by means of X-ray powder diffraction (XRD).

## 3. Results and discussion

### 3.1. Bottom ash components

The composition of the bottom ash was determined by XRD in conjunction with the microscopic analysis of thin and polished sections. Bottom ash components were essentially divided into six different groups of components:

- Crystalline silicates in a glass matrix: hedenbergite (Fig. 4), ferrohedenbergite, melilite, wollastonite, quartz, feldspar (both as well as rounded grains with many fissures and cracks).
- Oxides, sometimes in siliceous glass matrix: magnetite (Fig. 5), hematite, periclase.
- Bottle glass, mostly composed of $Na_2O$, CaO and $SiO_2$ sometimes fused with quartz and feldspar.
- Metals: aluminium, brass, steel, copper, zinc.

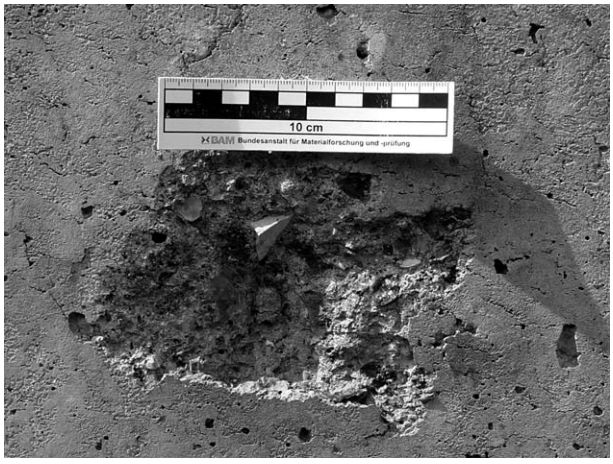


Fig. 2. Spalling on a face of the outdoor exposure specimen.

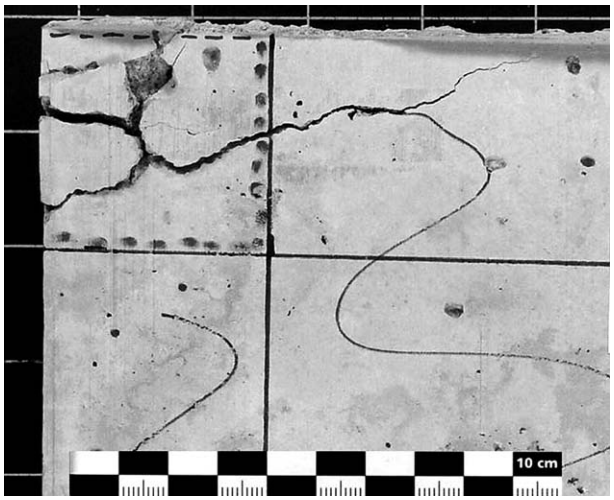


Fig. 3. Spalling of a corner at a cube of a laboratory sample.

- Ceramic fragments: china, brick, plaster, mortar.
- Components of organic origin: apatite (bone fragments), charcoal, plant fibres, polymers.

In general, the composition of bottom ash was very heterogeneous. Many other materials in addition to those listed above could be detected, but only occasionally, and in very low amounts. Iron oxides were usually embedded in a siliceous glass matrix but in particular magnetite could also appear together with hedenbergite or ferrohedenbergite. When bottle glass was fused with siliceous grain components (quartz, feldspar), in most cases, devitrification products were present in the glass matrix nearby or in direct contact with the grains.

### 3.2. General microstructure of the concretes

The microstructure of the laboratory prepared, as well as the field concretes, was dominated by the high amount of large,


Fig. 4. Hedenbergite crystals in a MSWI bottom ash aggregate (photomicrograph, transmitted light, crossed Nichols).

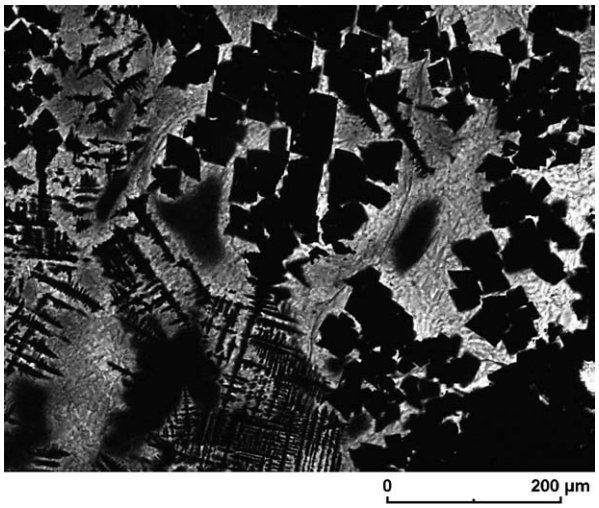


Fig. 5. Magnetite embedded in a siliceous glass matrix (photomicrograph, transmitted light).

irregular formed voids. The voids caused the typical pitted and cratered appearance on the outside surface of the concrete specimens. Under the microscope three different types of voids could be recognized (Fig. 6):

a. Nearly spherical voids similar to those found in normal concretes.
b. Linear arrangements of elongated voids with high length/width ratios. Those voids can be mistaken as cracks by naked eye observation.
c. Elongated voids, following the contours of grains (mostly aluminium).

Type b. and c. voids are not found in normal concretes. They are clearly linked to a reaction producing a gas phase during the plastic state of the cement binder. The only ash components, which are able to release larger amounts of hydrogen during a reaction in an alkaline environment, are metals like aluminium or zinc [24,2,17,25]. The voids formed by hydrogen release also contributed to the high porosity of concretes containing MSWI ash.

The concrete samples from the outdoor exposure always showed an irregular carbonation layer, with a minimum depth of 10 mm. At greater depths, larger voids were often observed under the microscope, surrounded by an isolated rim of carbonated cement paste. Obviously, in these cases, a system of voids similar to type b. in conjunction with cracks allowed atmospheric carbon dioxide to penetrate deep into the concrete. These void and crack systems are usually wider than 50 µm. Therefore they would easily facilitate the penetration of carbon dioxide to a depth greater than 50 mm, as discussed by St. John et al. [26].

### *3.3. Observed reactions of bottom ash components in the cement paste matrix*

Three different reactions were observed in the concrete specimens:

a. Alkali-silica reaction (ASR) of bottle glass fragments and glassy compounds of other siliceous components of the bottom ash.
b. Reaction of aluminium to form aluminium hydroxide and calcium aluminate hydrate (CAH).
c. Reaction of aluminate with calcium sulphate to form ettringite and monosulphate.

The expansive reaction of free lime or magnesium oxide to their hydrates was not observed in the samples.

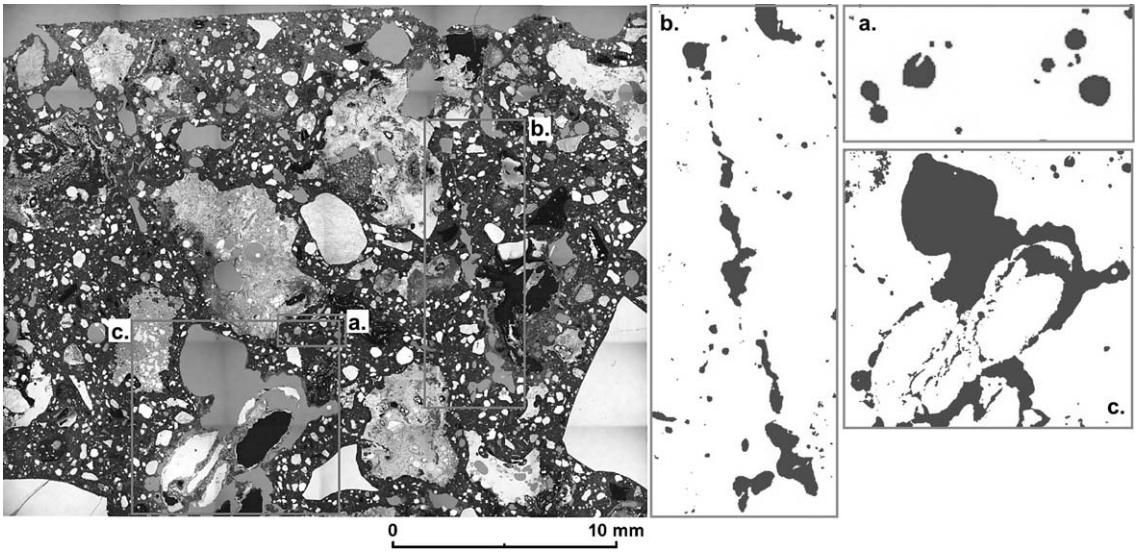


Fig. 6. Photomicrograph of the texture of an outdoor exposed concrete sample (transmitted light). On the right hand are the corresponding void types extracted from the photomicrograph by digital image analysis: a. Spherical voids; b. Elongated voids, which have a crack like macroscopic appearance; c. Voids around grains.

### 3.4. Alkali-silica reaction (ASR)

ASR occurred in the laboratory samples which were stored in the humidity chamber for 9 months as well as in the eight year old field concretes. The reaction was clearly linked to the fragments of bottle glass and the glassy silicates of the bottom ash. The chemical composition of bottle glass represented essentially a sodium calcium silicate glass but could deviate considerably from this composition. The gel formation often appeared inside the glass fragments leading to their partial disintegration as described in Ref. [27] and illustrated in Fig. 7. This internal gel formation was accompanied by many cracks, which were generated in the glass fragments after cooling of the bottom ash. The elemental composition of the gel was always rich in silica, calcium, potassium and sodium (Fig. 8). If sodium was present the K/Na-ratio was mostly greater than 1. Gel, with exclusively sodium as an alkali compound as described in Ref. [28], could not be found.

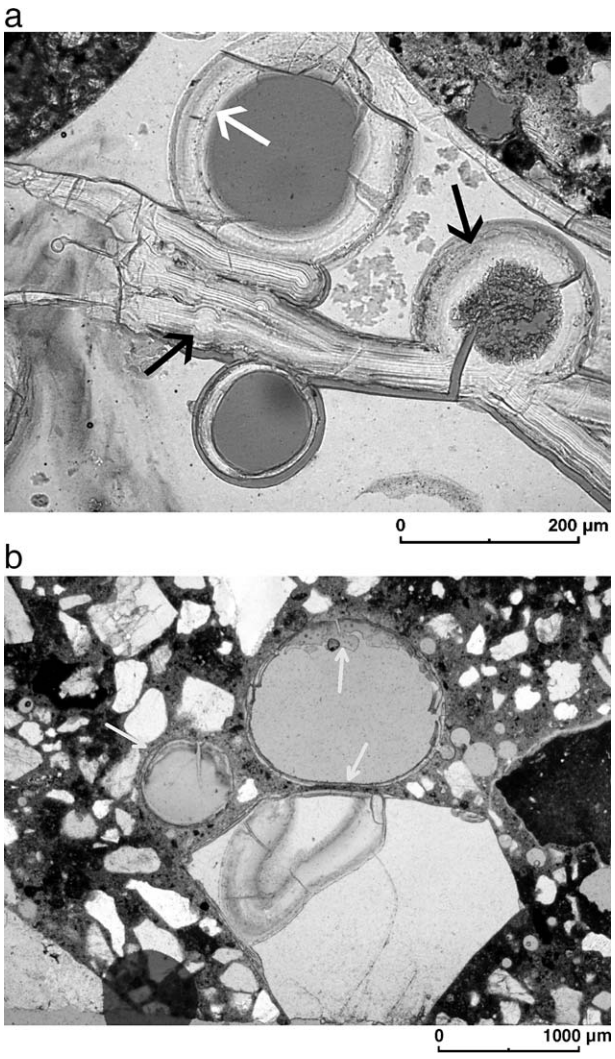


Fig. 7. a. Silicate gel inside a bottle glass fragment (arrows). Eight year old concrete. b. Silicate gel in- and outside (arrows) a glass fragment consisting of sodium oxide and silicon dioxide. Laboratory sample after 9 month in humidity chamber (photomicrographs, transmitted light).

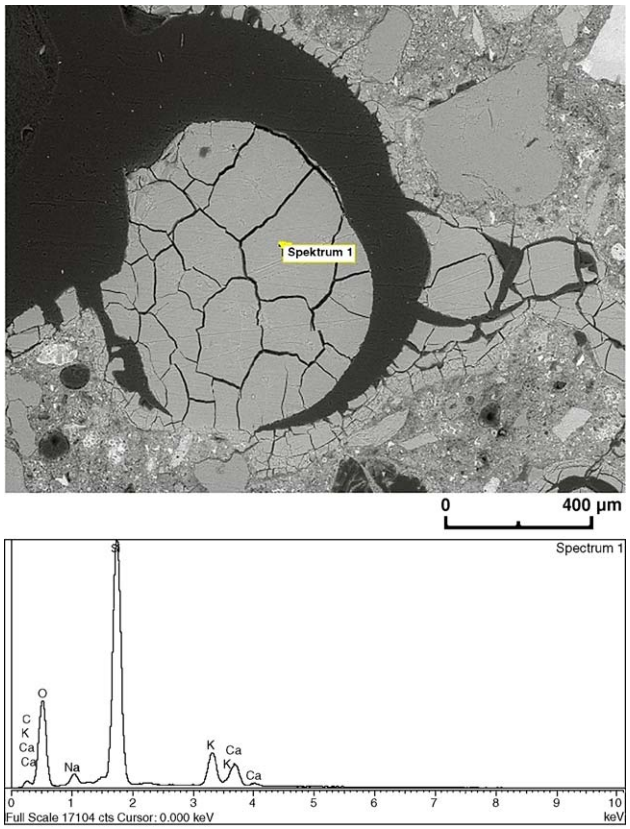


Fig. 8. Alkali-silica gel in a pore of a field concrete sample. The chemical composition is illustrated in the corresponding EDX spectrum (photomicrograph, SEM backscatter mode).

The field concrete samples showed no clear evidence of the deleterious action of gel expansion. Almost all of the silica gel found in the concretes appeared not on cracks but in large voids. Gel induced cracking of aggregates was not observed. Laboratory samples (moulded into bars and cubes) exposed in the humidity chamber showed only a negligible expansion during the recorded period of 9 months. Only one concrete bar exhibited a large ASR induced crack after the exposure period. In this case, the crack was clearly caused by a large agglomeration of bottle glass fragments, which were fused together with steel and other ash compounds (Fig. 9). Gel formation inside the bottle glass fragments was evident. The distribution of potassium showed that glass inside the agglomeration was transformed to a large degree, into a silicate gel, and was exclusively responsible for the crack formation (Fig. 9).

Problems with the loss of adhesion between the cement paste and fragments of bottle glass, due to leaching of the glass surface found by Winnefeld et al. [29] and Pickel [30], were not detected. It seemed that most of the alkali-silicate gel formed could be accommodated in the large pores and voids of the cement paste matrix, and, the aggregates themselves.

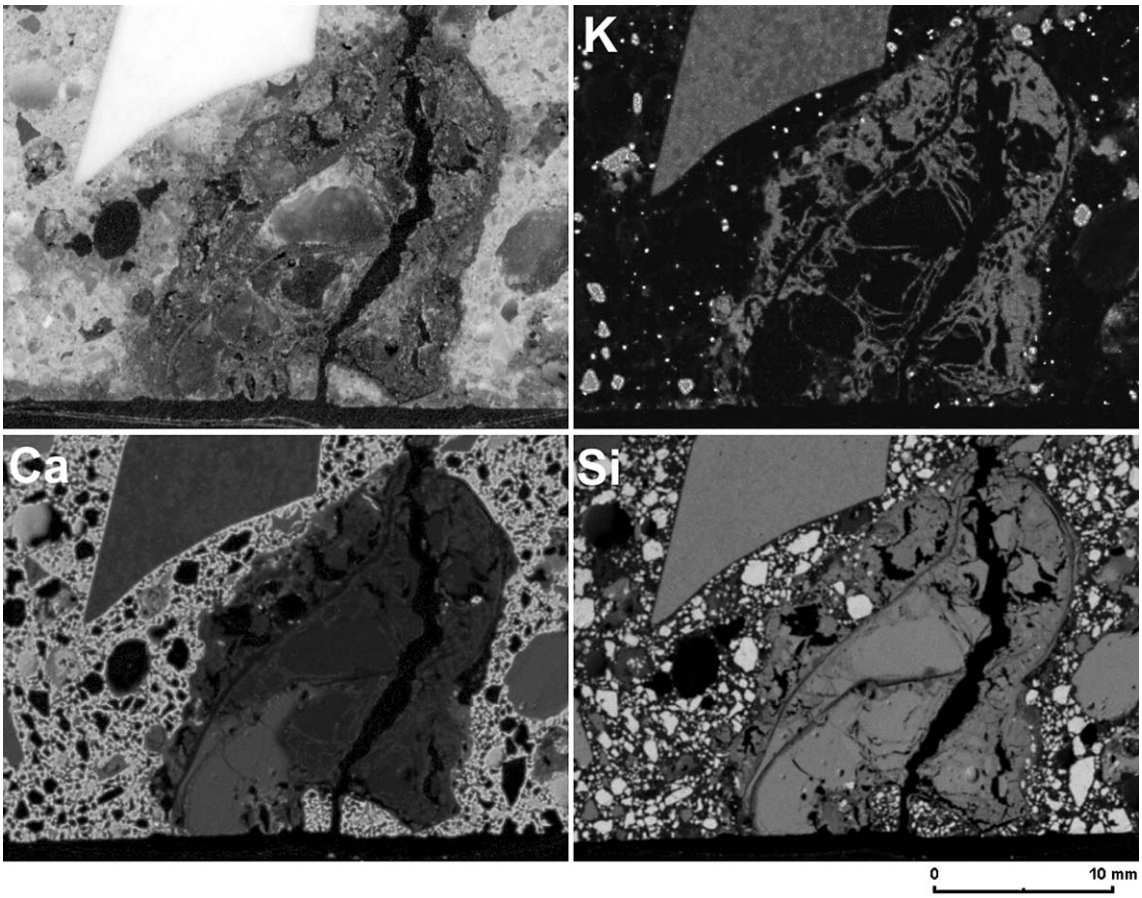


Fig. 9. Glass inclusion which caused cracking by expansion due to ASR (reflected light). Elemental distribution of calcium (Ca), potassium (K) and silicon (Si). The potassium distribution inside the inclusion represents the silica gel (EDX map from micro-XRF).

### 3.5. Reaction of aluminium with the cement matrix

The dominant reactions of the components of MSWI bottom ash in the cement paste matrix concerns the aluminium inclusions. The aluminium reacts to form aluminate in alkaline solutions (pH > 10) because the amphoteric $Al(OH)_3$ dissolves and does not form a passive layer (Eqs. (1)–(3)). The reaction is accompanied by a steady development of hydrogen gas

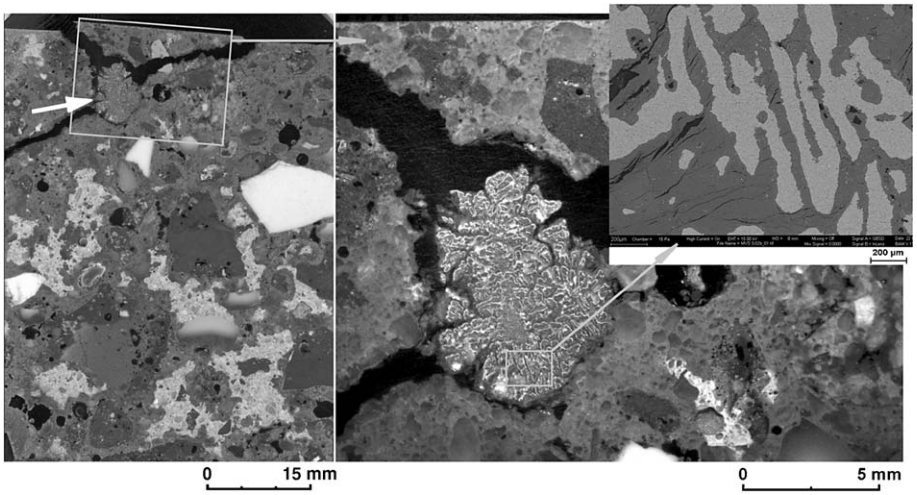


Fig. 10. Aluminum grain (arrow), which caused spalling of the corner of specimen in Fig. 3 (polished cross section, reflected light). The inset image shows a SEM image of the intergrowth of aluminum and aluminum hydroxide.

(reaction 1). At pH = 9 to 10 a $Al(OH)_3$ gel precipitates because it falls below the solubility product.

$$Al + 2OH^- + H_2O \rightarrow [AlO(OH)_2]^- + H_2 \uparrow \quad pH > 7 \qquad (1)$$

$$[AlO(OH)_2]^- + H_2O \rightarrow Al(OH)_3 + OH^- \quad pH = 9 - 10 \qquad (2)$$

$$Al(OH)_3 + OH^- \rightarrow [Al(OH)_4]^- \quad pH > 10 \qquad (3)$$

The reactions of aluminium could be observed in all laboratory and field concretes. The spalling illustrated in Figs. 2 and 3 occurred due to aluminium reactions in the hardened concrete. Fig. 10 shows the aluminium grain which caused the spalling in Fig. 3. The reaction products exerting expansive forces, consisted mainly of aluminium hydroxide, and exhibited a distinctive pattern of intergrowth with aluminium (Fig. 10).

It might be possible that the $OH^-$ concentration in the hardened cement paste matrix surrounding the reacting aluminium metal fragments decreases as a consequence of the reactions (Eqs. (1)–(3)), in conjunction with the low diffusivity of $OH^-$ ions in the paste. This would allow the formation of aluminium hydroxide, in the near vicinity of the aluminium grain.

Aluminium hydroxide appeared in three different phases: amorphous $Al(OH)_3$ and in the two crystalline modifications bayerite ($\alpha$-$Al(OH)_3$) and boehmite ($\gamma$-AlOOH), which were confirmed by XRD analysis. The amorphous modification was clearly gel like (Fig. 11a), and sometimes it was only possible to differentiate from silicate gel by microchemical analysis. Bayerite appeared sometimes in well-formed plate like crystal aggregates inside pores (Fig. 11b), but was mostly aggregated in compact masses. SEM analysis revealed that amorphous aluminium hydroxide surrounding the aluminium grain was often succeeded by a second layer of crystalline Al-hydroxide

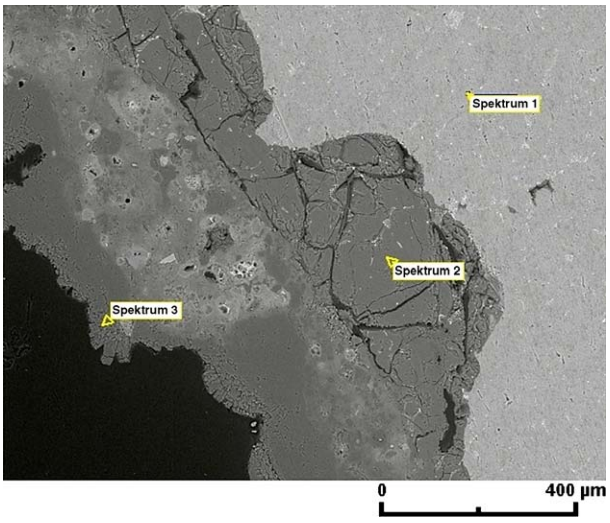


Fig. 12. Succession of aluminum metal (spectrum 1), a layer of cracked amorphous Al-hydroxide (spectrum 2) and a compact layer of crystalline Al-hydroxide (spectrum 3). SEM photomicrographs, backscatter.

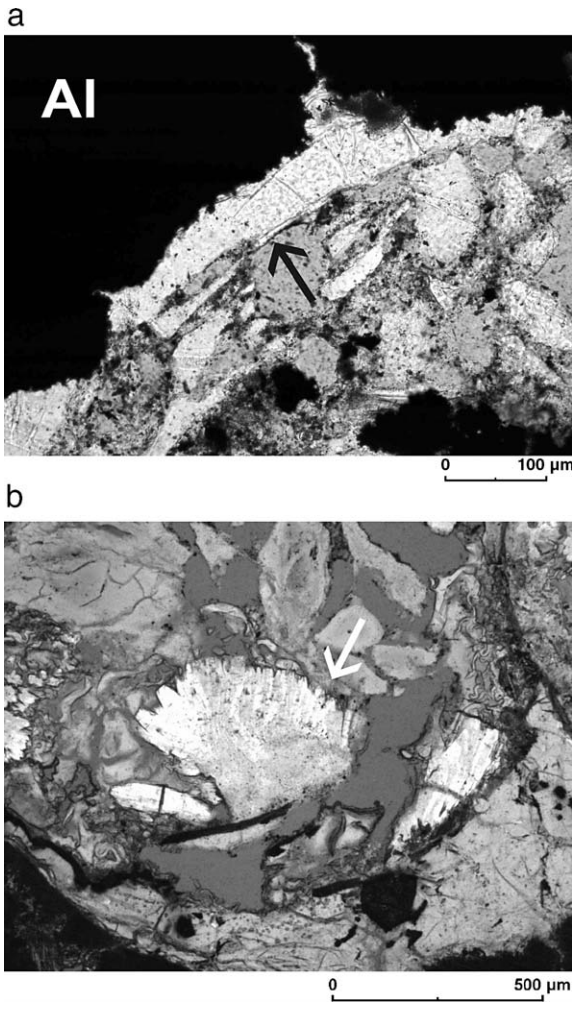


Fig. 11. a. Amorphous aluminum hydroxide (arrow) surrounding an aluminum grain (Al). b. Crystals of bayerite (arrow) in a pore with amorphous aluminum hydroxide (photomicrographs, transmitted light).

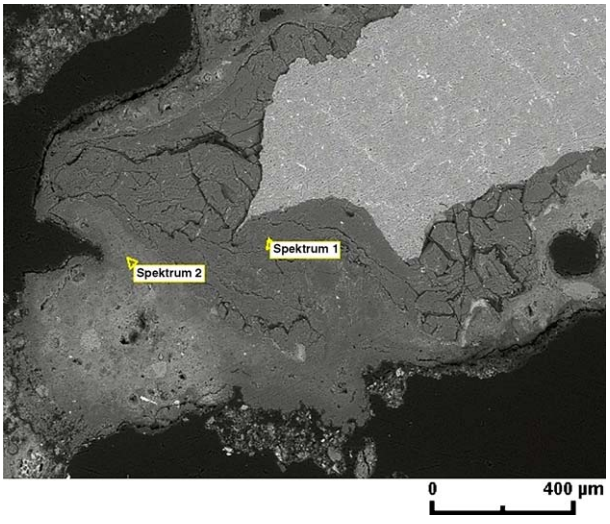


Fig. 13. An amorphous Al-hydroxide layer (spectrum 1) surrounding an aluminum grain (al) is followed by a calcium aluminate hydrate (spectrum 2). SEM photomicrographs, backscatter.

(Fig. 12)). The crystalline aluminium hydroxide was sometimes substituted by, or inter-grown with, amorphous calcium aluminate hydrate (Fig. 13). However, CAH phases appeared only in small amounts.

Aluminium always exhibited a reaction rim of aluminium hydroxide in the cement paste matrix. If a large number of large aluminium grains converted to hydroxide, and only if these metal grains were near the surface, damage in the form of spalling occurred. The expansive reaction due to aluminium occurred in the eight year old field concrete samples stored outdoors as well as in the laboratory samples during storage under water.

### 3.6. Reaction of aluminate with calcium sulphate

Reactions of aluminates with sulphate could only be detected in one sample. However, the complex layers of ettringite around aluminium inclusions described by Dreesen and Laenen [31] and Pecqueur et al. [2], could not be observed. This might be due to the fact that the sulphate concentration in the MSWI bottom ash was below 1 M-%. In a single case a grain consisting of a sulphate-rich old mortar, which was a component of the bottom ash, reacted with aluminate to form ettringite (Fig. 14). Ettringite appeared in cracks inside the mortar grain as irregular masses, and in pores sometimes in the form of acicular crystals (Fig. 15). These examples show that the reaction leading to the formation of ettringite occurs if a source of sulphate is in close proximity to an aluminium grain.

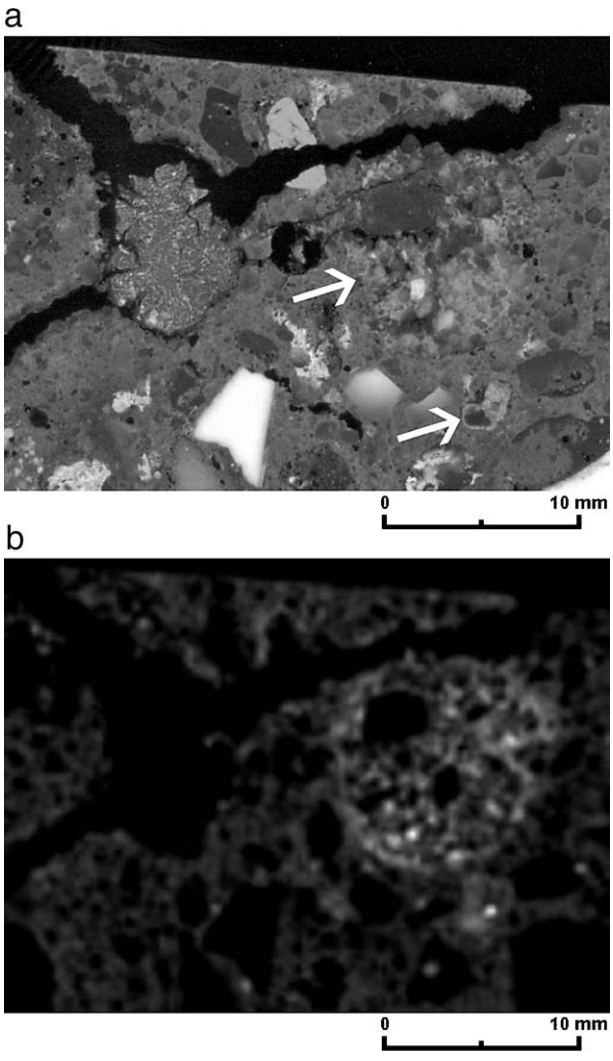


Fig. 14. a. Polished cross section of the sample from Fig. 10. The arrows indicate old mortar grains embedded in the cement paste. b. Elemental map of sulfur of the area of a. An enrichment of sulfur is visible in the location of the old mortar grains.

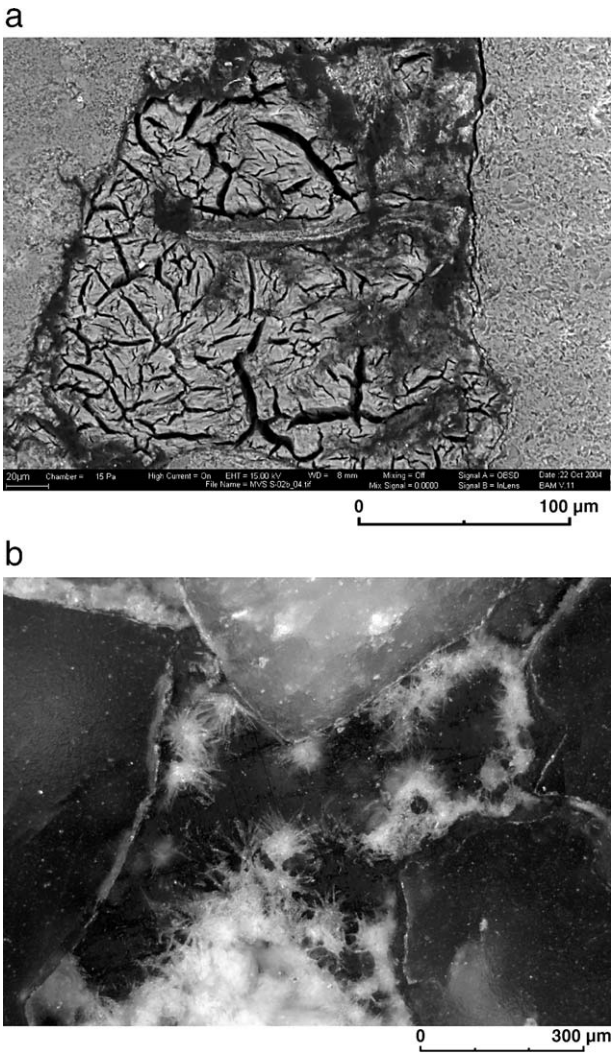


Fig. 15. Inside the mortar grains ettringite was formed in the form of irregular masses on cracks (a.) or as acicular crystals in pores (b.) (SEM, backscatter image and photomicrograph in reflected light).

## 4. Conclusions

The main mechanism affecting the durability of concrete made with MSWI bottom ash as an aggregate component is the reaction of aluminium with the cement paste to form aluminium hydroxide, aluminates and hydrogen. If moisture is present, the reaction is able to proceed long after har-

dening of the concrete. If the reaction occurs in the near surface region in conjunction with a high reaction rate, spalling will take place.

A secondary problem arises with the susceptibility of the glass components of the bottom ash to ASR. The potential of silicate gel formation is inherent in the outdoor exposed field samples as well as in the laboratory concretes. Actual damage due to ASR was sporadic even though abundant silicate gel formation was observed in all sample specimens. Obviously the high porosity of the bottom ash aggregates together with the additional open void space (due to release of $H_2$ from the aluminium reaction in the cement paste matrix) allowed not only newly formed silicate gel, but also aluminium hydroxide, to form in the pore space (to a certain degree) without exerting any stress on the cement paste or aggregate.

The reduction of the aluminium content is the first requirement to new processing technologies. If it is possible to reduce the aluminium content and, to lower the porosity of the concrete, ASR will become a more prominent reaction as reported in the literature concerning waste glass as aggregates in concrete [28–30,32]. To guarantee durability for concrete made with MSWI bottom ash, additional processing technologies must therefore be pursued, which allow firstly to reduce the aluminium content of the MSWI bottle ash and secondly to reduce the amount of bottle glass.

## Acknowledgements

The authors would like to especially thank the *MVR Müllverwertung Rugenberger Damm GmbH and Co KG* for financing the project and for their logistic support, Martin K. Head, Imperial College London, for reviewing the manuscript and our colleague Frank Haamkens for his responsible realization of the production and testing of the laboratory concretes. Without the efforts and patience of our colleagues Romeo Saliwan-Neumann and Gerd Nolze the SEM-analysis would not have been possible; many thanks for their support.

## References

[1] A.R. Hill, A.R. Dawson, M. Mundy, Utilization of aggregate materials in road construction and bulk fill, Resources, Conservation and Recycling 32 (3–4) (2001) 305–320.
[2] G. Pecqueur, C. Crignon, B. Quenee, Behaviour of cement-treated MSWI bottom ash, Waste Management 21 (3) (2001) 229–233.
[3] J. Reichelt, G. Pfrang-Stotz, Technical properties and environmental compatibility of MSWI bottom ashes and other industrial by-products used as recycled materials in road construction, IT3 Conference 'Incineration and Thermal Treatment Technologies', New Orleans, Louisiana, 2002.
[4] R. Forteza, M. Far, C. SeguI, V. Cerda, Characterization of bottom ash in municipal solid waste incinerators for its use in road base, Waste Management 24 (9) (2004) 899–909.
[5] P. Appendino, M. Ferraris, I. Matekovits, M. Salvo, Production of glass-ceramic bodies from the bottom ashes of municipal solid waste incinerators, Journal of the European Ceramic Society 24 (5) (2004) 803–810.
[6] L. Bertolini, M. Carsana, D. Cassago, A. Quadrio Curzio, M. Collepardi, MSWI ashes as mineral additions in concrete, Cement and Concrete Research 34 (10) (2004) 1899–1906.
[7] P. Filipponi, A. Polettini, R. Pomi, P. Sirini, Physical and mechanical properties of cement-based products containing incineration bottom ash, Waste Management 23 (2) (2003) 145–156.
[8] A. Polettini, R. Pomi, G. Carcani, The effect of Na and Ca salts on MSWI bottom ash activation for reuse as a pozzolanic admixture, Resources, Conservation and Recycling In Press, Corrected Proof.
[9] D. Traber, U.K. Mäder, U. Eggenberger, Petrology and geochemistry of a municipal solid waste incinerator residue treated at high temperature, Schweizerische Mineralogische und Petrographische Mitteilungen 82 (2002) 1–14.
[10] K.O. Ampadu, K. Torii, Characterization of ecocement pastes and mortars produced from incineration ashes, Cement and Concrete Research 31 (2001) 431–436.
[11] H. Hirao, S. Yokoyama, Behavior of chloride ions in hardened eco-cement: a new type of Portland cement made from municipal waste incinerator ash, in: G. Owens, G. Grieve (Eds.), 11th International Congress on the Chemistry of Cement, Durban, South Africa, Cement and Concrete Institute of South Africa, 2003, pp. 1271–1281.
[12] T. Shimoda, S. Yokoyama, H. Hirao, Eco-cement: A new Portland cement to solve municipal and industrial waste problems, Teiheiyo Semento Kenyu Hokoku 138 (2000) 5–15.
[13] C.A. Sikalidis, A.A. Zabaniotou, S.P. Famellos, Utilization of municipal solid wastes for mortar production, Resources, Conservation and Recycling 36 (2) (2002) 155–167.
[14] K. Torii, H. Tomotake, K.O. Ampadu, T. Echigo, Compatibility between ecocement produced from incinerator ash and reactive aggregates in ASR expansion of mortars, Cement and Concrete Research 33 (4) (2003) 571–577.
[15] L. Courard, R. Degeimbre, A. Darimont, A.-L. Laval, L. Dupont, L. Bertrand, Utilisation des mâchefers d'incinérateur d'ordures ménagères dans la fabrication de pavés en béton, Materials and Structures 35 (2002) 365–372.
[16] M. Schmidt, Verwertung von Müllverbrennungsrückständen zur Herstellung zementgebundener Baustoffe, Beton 38 (6) (1988) 238–245.
[17] J. Pera, L. Coutaz, J. Ambroise, M. Chababbet, Use of incinerator bottom ash in concrete, Cement and Concrete Research 27 (1) (1997) 1–5.
[18] F. Pilny, W. Hiese, Schwer- und Leichtbeton aus Müll-Schlackensinter, Die Bautechnik 7 (1967) 230–238.
[19] DIN EN 1744-1, Prüfverfahren für chemische Eigenschaften von Gesteinskörnungen, Teil 1: Chemische Analyse, Deutsche Norm, Beuth Verlag, Berlin, 1998.
[20] DAfStb, Vorbeugende Maβnahme gegen schädigende Alkalireaktion im Beton (Alkali richtlinie), DAfStb-Richtlinie, Deutscher Ausschuss für Stahlbeton (DAfStb), Berlin, 2001.
[21] J.M. Chimenos, M. Segarra, M.A. Fernandez, F. Espiell, Characterization of the bottom ash in municipal solid waste incinerator, Journal of Hazardous Materials 64 (3) (1999) 211–222.
[22] B. Hentschel, Vergleichende mineralogische und chemische Untersuchungen an Rostschlacken aus Anlagen zur thermischen Abfallbehandlung, Berichte aus der Umwelttechnik, Shaker, Aachen, 1999.
[23] U. Müller, The micro-XRF — a new technique for the analysis of building materials, Construction Technology in Europe 26 (2004) 3–4.
[24] A.F. Hollemann, E. Wiberg, N. Wiberg, Lehrbuch der anorganischen Chemie, Walter de Gruyter, Berlin, New York, 1995.
[25] J.M. Chimenos, A.I. Fernandez, R. Nadal, F. Espiell, Short-term natural weathering of MSWI bottom ash, Journal of Hazardous Materials 79 (3) (2000) 287–299.
[26] D.A. St. John, A.B. Poole, I. Sims, Concrete petrography: A Handbook of Investigative Techniques, John Wiley & Sons, New York, 1998.
[27] A. Mladenovic, J.S. Suput, V. Ducman, A.S. Skapin, Alkali-silica reactivity of some frequently used lightweight aggregates, Cement and Concrete Research 34 (10) (2004) 1809–1816.
[28] A. Shayan, A. Xu, Value-added utilization of waste glass in concrete, Cement and Concrete Research 34 (1) (2004) 81–89.

[29] F. Winnefeld, E. Warianka, D. Knöfel, Dauerhaftigkeit von Recyclingglas als Zuschlag in Beton in Abhängigkeit von der Rezeptur, In: F.H. Wittmann, A. Gerdes (eds.), Material Science and Restoration V, Vol. 2 of 2, Esslingen, Germany, Aedificatio, Freiburg, (1999), 1619–1630.
[30] U. Pickel, Glaseinstreuungen in Betonwerkstein, Betonwerk und Fertigteil-Technik 58 (1992) 56–58.
[31] R. Dreesen, B. Laenen, D. Wan Rossem, Aggregate-cement reactions in MSWI-bottom ash based concrete — a petrographic assesment, in: M. Stamatakis, B. Georgali, D. Fragoulis, E.-E. Toumbakari (Eds.), Proceedings of the 8th Euroseminar on Microscopy Applied to Buildings Materials, 2001, pp. 113–120, Athens, Greece.
[32] V. Ducman, A. Mladenovic, J.S. Suput, Lightweight aggregate based on waste glass and its alkali-silica reactivity, Cement and Concrete Research 32 (28) (2002) 223–226.